Non-Ideal Proportional Resonant Control for Modular Multilevel Converters under Sub-Module Fault Conditions

Hu, Pengfei; He, Zhengxu; Li, Shuqi; Guerrero, Josep M.

Published in:
IEEE Transactions on Energy Conversion

DOI (link to publication from Publisher):
10.1109/TEC.2019.2938395

Publication date:
2019

Document Version
Accepted author manuscript, peer reviewed version

This article has been accepted for publication in a future issue of this journal, but has not been fully edited. Content may change prior to final publication. Citation information: DOI 10.1109/TEC.2019.2938395, IEEE Transactions on Energy Conversion

Non-Ideal Proportional Resonant Control for Modular Multilevel Converters under Sub-Module Fault Conditions

Pengfei Hu, *Member, IEEE,* Zhengxu He, Shuqi Li, and Josep M. Guerrero, *Fellow, IEEE*

Nomenclature

The upper and lower arms of the MMC are denoted with the subscripts "*u*" and "*l*", respectively. The phase number is denoted with the subscript "*j*".

u_{ca}	Converter-side AC voltage of phase *a*.
$u_{ua,la}$	Arm voltages of phase *a*.
$\bar{u}_{ua}$, $\tilde{u}_{ua}$	DC and AC components of the upper-arm voltage of phase *a*.
$\bar{u}_{la}$, $\tilde{u}_{la}$	DC and AC components of the lower-arm voltage of phase *a*.
I_{ua}, I_{la}	DC amplitudes of the arm currents of phase *a*.
I_{mua}, I_{mla}	Amplitudes of the fundamental components of the arm currents of phase *a*.
U_{dc}	Pole-to-pole DC bus voltage.
i_a	AC current of phase *a*.
$i_{ua,la}$	Arm currents of phase *a*.
i_{cira}	Circulating current of phase *a*.
$\tilde{i}_{cira}$	AC components of the circulating current of phase *a*.
u_{sa}	Grid-side AC voltage of phase *a*.
I_{dc}	DC current.
N	Total number of SMs per arm.
U_d	Rated average capacitor voltage.
$u_{SMua,SMla}$	Output voltage of the sub-module (SM) in the upper or lower arm of phase *a*.
$u_{cua,cla}$	Capacitor voltage of the SM in the upper or lower arm of phase *a*.
N_r	Number of redundant SMs per arm.
C	SM capacitance.
L_0	Arm inductance.
R_0	Equivalent arm resistance.
L	AC inductance.
R	Equivalent AC line resistance.
m	Modulation index (ranging from 0–1).
$S_{ua,la}$	Average switching function of an arbitrary sub-module in the upper or lower arm of phase *a*.
$N_{ua,la}$	Number of the inserted SMs of the upper or lower arm of phase *a*.

***Abstract*—The Modular Multilevel Converter (MMC) has become the most promising topology for high-voltage and high-power applications. Sub-Module (SM) fault ride-through capability is one of the most important features of the MMC. To study the approach of controlling SM faults, the differences between hot-backup and cold-backup configuration of redundant SMs are analyzed. After that, an internal asymmetrical dynamic model for the MMC is analyzed, which shows that unexpected fundamental and 3rd harmonic components in the circulating current result in fluctuation of DC current. Based on this model and by integrating the conventional circulating current suppression method and the SM-fault tolerant approach, a non-ideal proportional-resonant (PR) controller is proposed and analyzed. This control scheme can suppress the fluctuation of the DC current of the MMC under SM faults without the knowledge of the number of faulty SMs and extra communication system. Its effectiveness is verified by both PSCAD/EMTDC simulations and scaled-down prototype experiments.**

***Index Terms*—Modular Multilevel Converter (MMC); sub-module (SM) faults; proportional resonant control; redundant sub-modules.**

I. Introduction

The modular multilevel converter (MMC) has become the most popular topology for high-voltage and high-power applications due to its high efficiency, excellent output performance, scalability and capability of efficient fault management [1]–[5]. With these advantages, it becomes a promising candidate for high-voltage direct-current (HVDC) transmission [6]–[8], transformer-less static synchronous compensators (STATCOM) [9]–[10], high-power motor drives [11]–[13] and electric railway supplies [14].

Different from the two-level converter, the MMC can generate the desired voltages through cascaded sub-modules in each arm, which is the reason why MMCs have distinctive

Manuscript revised

Corresponding authors: Zhengxu He and Pengfei Hu.

Pengfei Hu is with School of Mechanical and Electrical Engineering, University of Electronic Science and Technology of China, Chengdu, 611731, China (E-mail: pfhu@uestc.edu.cn).

Zhengxu He is with Sichuan Energy Internet Research Institute, Chengdu, 610213, China (xuzonehe@126.com)

Shuqi Li is with State Grid Sichuan Electric Power Research Institute, Chengdu, China, (lishuqi1990@qq.com).

Josep M. Guerrero is with Department of Energy Technology, Aalborg University, Aalborg, Denmark (joz@et.aau.dk).

characteristics. One critical issue of the MMC that has attracted much attention is capacitor-voltage balancing [15]–[17]. Modeling of MMCs has also been widely investigated by [18]–[21], including steady-state modeling, dynamic modeling and frequency-domain modeling. Of all research focus, the control methods of the circulating currents caused by the distinctive internal dynamics have drawn the most attention of scholars and engineers. The concept of circulating current was firstly proposed in [22]. The mechanism of three-phase circulating currents in the MMC was analyzed in [23], and the relationship between the amplitudes of circulating currents and the parameters of arm inductors was discussed in [24]. Later on, there appeared numerous control methods of circulating currents under balanced and unbalanced grid voltages. Reference [25] proposed a rotating dq-frame-based circulating current suppressing method under balanced grid voltages. Regarding unbalanced grid-voltage conditions, [26] and [27] proposed similar PR controllers to suppress the positive-sequence and negative-sequence circulating current components. The proposed methods were validated solely by simulation results, and neither presents parameters tuning procedures. Reference [26] focused on the analysis and control of the unbalanced 2nd harmonic components of circulating current caused by the unbalanced grid voltages, without considering the unbalanced fundamental and 3rd harmonic components caused by the sub-module faults. Similarly, reference [27] proposed a positive and negative sequence decomposition based non-ideal PR controller to regulate the output AC current and circulating currents in the AC grid unbalanced condition. Besides, repetitive controllers were employed in [28] and [29] to suppress the 2nd harmonic component of the circulating current. Both papers investigated the repetitive controller applied in the MMC under ideal conditions (both AC grid and internal dynamic symmetry conditions). Additionally, reference [28] used the carrier phase shifted pulse width modulation, which is only suitable for the MMC containing small numbers of sub-modules. Moreover, reference [30] employed the redundant sub-modules to generate redundant voltage levels to mitigate the inherent 2nd harmonic component in the circulating current, which can be regarded as an indirect control method. Compared with other direct control of circulating current, the indirect way is simpler implementation with the sacrifice of precision. Unlike the relative references, this paper focuses on the internal dynamic of the MMC, especially the sub-module faults. The harmonic components of the circulating currents are different from those in the AC grid fault conditions. Meanwhile, the proposed method can realize the fluent transition when sub-module fault happens without the knowledge of the faulty sub-module number.

On the other hand, since the MMC is composed of hundreds of sub-modules (SMs) in high-voltage applications, the operation status of each SM will affect the overall performance of the MMC. Therefore, the SM-fault control strategy is another critical issue of the MMC control. Recently, the control and ride-through strategies regarding this issue have been proposed in a few papers, including fault diagnosis strategies using additional circuits or devices [31] and open-circuit fault detection methods using state observers [32]–[35]. Normally, hot-backup redundant SMs are configured in the main circuit, and faulty SMs are bypassed immediately after being located. Reference [36] proposed an energy-balancing control strategy to maintain internal dynamic symmetry under SM fault conditions, where the number of the faulty SMs needs to be given. Reference [37] proposed a PI-based controller under SM fault conditions; however, this controller has a complicated structure and tricky parameter tuning as it employs a band-pass filter, two notch filters, two PI controllers and an extra 2nd harmonic circulating current controller.

In order to simplify the structure of SM-fault controllers, this paper proposes a non-ideal PR controller integrating the conventional functions of 2nd-harmonic circulating current suppression and of SM-fault ride-through without the knowledge of the number of faulty SMs. The outline of this paper is organized as follows. Section II compares different configurations of redundant SMs. Section III presents the mathematical model of internal asymmetrical MMCs. In Section IV, the proposed non-ideal PR controller is analyzed. Section V and Section VI present simulation and experimental results to validate the proposed control strategy. Section VII concludes this paper.

II. CONFIGURATIONS OF REDUNDANT SMS

Normally, there are two types of configurations for redundant SMs.

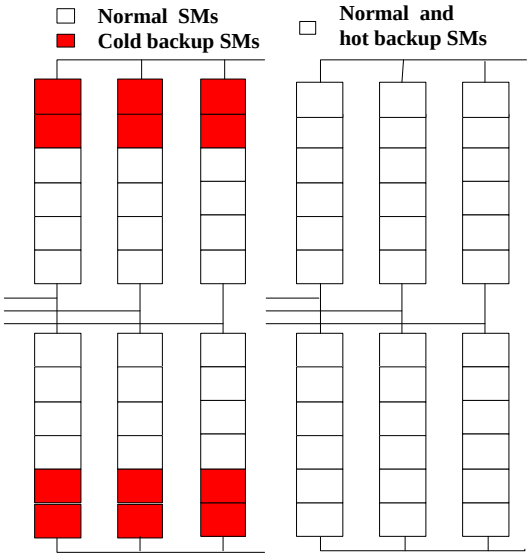

(a) Configuration 1 (b) Configuration 2

Fig.1 Configurations for redundant SMs

Configuration 1 (see Fig.1(a)): Redundant SMs are in cold backup, which means that they are bypassed by bypass switches. When SM faults occur, the faulty SMs must be located and bypassed immediately. Meanwhile, the same number of redundant SMs need to be activated, charging their capacitors to the rated voltages and then operating as normal SMs [38].

Configuration 2 (see Fig.1(b)): Redundant SMs are in hot

This article has been accepted for publication in a future issue of this journal, but has not been fully edited. Content may change prior to final publication. Citation information: DOI 10.1109/TEC.2019.2938395, IEEE Transactions on Energy Conversion

backup, which means that they operate in the same way as the normal ones. When SM faults occur, two strategies can be adopted: one (called Configuration 2A) is to bypass the faulty SMs as well as the same number of SMs in the healthy arms to keep the system symmetrical, and the other option (called Configuration 2B) is to merely bypass the faulty SMs, making the system operate in an unbalanced condition.

In Configuration 1, such drawbacks as high cost, complex control system and long charging time of redundant SMs exist. On the other hand, the reliability of Configuration 2A is lower than that of Configuration 2B, as extra normal SMs are bypassed under SM fault conditions. Therefore, as a more economic and reliable scheme, Configuration 2B is adopted in this paper. It is notable that this scheme does have a disadvantage that the MMC has to work under unbalanced conditions. To resolve this issue, a mathematical model for MMCs with the arms containing different numbers of SMs will be studied in Section III.

III. Mathematical Model for Asymmetrical MMCs

A. Basics of MMCs

As shown in Fig.2, a three-phase MMC consists of six arms, each of which is composed of N identical SMs and an arm inductor L_0 (R_0 denotes the equivalent arm resistance). The operation status of a sub-module is illustrated in Table I. The operating principles of the MMC have been studied by many previous papers. Hence, only the basic internal relationship is given here. The AC-side output voltage and current of the MMC are given by equations (1) and (2), respectively. The relationship among arm current, AC current and circulating current is demonstrated by equation (3).

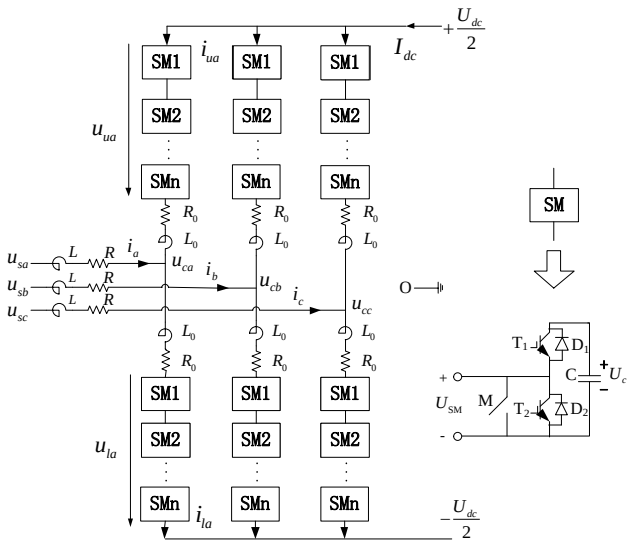

Fig.2 Circuit topology of an MMC

$$u_{cj} = \frac{mU_{dc}}{2}\sin(\omega t) \tag{1}$$

$$i_j = I\sin(\omega t - \varphi) \tag{2}$$

$$\begin{cases} i_{uj} = -\dfrac{1}{2}i_j + i_{cirj} \\ i_{lj} = \dfrac{1}{2}i_j + i_{cirj} \end{cases} \tag{3}$$

TABLE I
Operation Status of a Half-Bridge SM

SM Status	T_1	T_2	U_{SM}	Arm Current	Charging State
Inserted	on	off	U_c	Positive	Charging
	on	off	U_c	Negative	Discharging
Bypassed	off	on	0	Positive or Negative	Unchanged
Blocked	off	off	U_c	Positive	Charging
	off	off	*0*	Negative	Unchanged

B. Dynamics of asymmetrical MMCs

To design the SM-fault controller, the dynamics of asymmetrical MMCs need to be analyzed first. According to [34] and [36], the basic operating principles are illustrated below. Since the principles are identical in three phases, phase *a* is taken as an example. The average switching functions of an arbitrary sub-module in the upper and lower arms of phase *a* can be defined as

$$\begin{cases} s_{ua} = \dfrac{1 - m\sin(\omega t)}{2} \\ s_{la} = \dfrac{1 + m\sin(\omega t)}{2} \end{cases} \tag{4}$$

According to capacitor dynamics, the following equations can be obtained:

$$\begin{cases} C\dfrac{du_{cua}}{dt} = s_{ua}i_{ua} \\ C\dfrac{du_{cla}}{dt} = s_{la}i_{la} \end{cases} \tag{5}$$

$$\begin{cases} u_{SMua} = s_{ua}u_{cua} \\ u_{SMla} = s_{la}u_{cla} \end{cases} \tag{6}$$

Due to the approach of balancing capacitor voltages [6], the SMs of the same arm can be regarded as having the same behavior. Therefore, the overall voltage of one arm can be calculated by

$$\begin{cases} u_{ua} = N_{ua}u_{SMua} = \bar{u}_{ua} + \tilde{u}_{ua} \\ u_{la} = N_{la}u_{SMla} = \bar{u}_{la} + \tilde{u}_{la} \end{cases} \tag{7}$$

Given that there are only DC and fundamental components in the arm currents, the arm currents can be given by

$$\begin{cases} i_{ua} = I_{ua} + I_{mua}\sin(\omega t + \alpha) \\ i_{la} = I_{la} + I_{mla}\sin(\omega t + \beta) \end{cases} \tag{8}$$

Combining (4)–(8), the AC components of the arm voltages are expressed by equations (9) and (10). As can be seen, the AC components are composed of fundamental, 2nd and 3rd harmonic components.

This article has been accepted for publication in a future issue of this journal, but has not been fully edited. Content may change prior to final publication. Citation information: DOI 10.1109/TEC.2019.2938395, IEEE Transactions on Energy Conversion

$$\tilde{u}_{ua}=\frac{N_{ua}}{2C}[\underbrace{-\frac{m+8}{16}I_{mua}\cos(\omega t+\alpha)+\frac{mI_{ua}}{2}\cos(\omega t)}_{\text{Fundamental component}} \underbrace{+\frac{3m}{8}I_{mua}\sin(2\omega t+\alpha)-\frac{m^2I_{ua}}{4}\sin(2\omega t)}_{\text{2nd harmonic component}}+\underbrace{\frac{m^2}{16}I_{mua}\cos(3\omega t+\alpha)}_{\text{3rd harmonic component}}] \tag{9}$$

$$\tilde{u}_{la}=\frac{N_{la}}{2C}[\underbrace{+\frac{m+8}{16}I_{mla}\cos(\omega t+\beta)-\frac{mI_{la}}{2}\cos(\omega t)}_{\text{fundamental component}} \underbrace{+\frac{3m}{8}I_{mla}\sin(2\omega t+\beta)-\frac{m^2I_{la}}{4}\sin(2\omega t)}_{\text{2nd harmonic component}}-\underbrace{\frac{m^2}{16}I_{mla}\cos(3\omega t+\beta)}_{\text{3rd harmonic component}}] \tag{10}$$

Applying Kirchhoff's voltage law, the following equations can be derived as

$$\begin{cases}\frac{1}{2}U_{dc}-u_{ca}=u_{ua}+L_0\frac{di_{ua}}{dt}+R_0i_{ua}\\ \frac{1}{2}U_{dc}+u_{ca}=u_{la}+L_0\frac{di_{la}}{dt}+R_0i_{la}\end{cases} \tag{11}$$

Summing the two equations of (11), the internal dynamic model of the MMC is derived as

$$L_0\frac{di_{cira}}{dt}+R_0i_{cira}=\frac{1}{2}U_{dc}-\frac{1}{2}(u_{ua}+u_{la}) \tag{12}$$

where $i_{cira}=0.5(i_{ua}+i_{la})$ denotes the circulating current of phase *a*. Substituting (9) and (10) into (12), it is obvious that if N_{ua} is not equal to N_{la} (i.e. the arms are unbalanced), $u_{ua}+u_{la}$ consists of DC, fundamental, 2nd and 3rd harmonic components. Accordingly, the circulating current also consists of these components. In contrast, there are only DC and 2nd harmonic components in the circulating current of the healthy phases. Thus, the asymmetry gives rise to fundamental frequency fluctuation of the DC current. To eliminate the fluctuation of DC current and to reduce losses, fundamental, 2nd and 3rd harmonic components need to be eliminated. The AC components of equation (12) can be rewritten as

$$L_0\frac{d\tilde{i}_{cira}}{dt}+R_0\tilde{i}_{cira}=-\frac{1}{2}(\tilde{u}_{ua}+\tilde{u}_{la})=u_{diff} \tag{13}$$

Hence, controllers are required to have the function of suppressing the fundamental, 2nd and 3rd harmonic components of the circulating current under SM fault conditions.

IV. Proposed Non-ideal PR Control Strategy

A. Basics of non-ideal PR controllers

The transfer functions of ideal and non-ideal PR controllers are illustrated by (14) and (15), respectively. The bode plots of the two PR controllers are shown in Fig.3. An ideal PR controller gives an infinite gain at the resonant frequency ω_n and no gains at other frequencies (red line in Fig.3). However, an ideal PR is quite sensitive to the accuracy of resonant frequency, and its infinite gain may cause stability problem. A non-ideal PR controller given by equation (15) is much more popular in practical applications. The non-ideal PR controller has a finite gain at the resonant frequency (blue line in Fig.3), but the gain is high enough to minimize small steady-state error. In (15), k_p is tuned in the same way as that for a PI controller, and determines the dynamics of the system in terms of bandwidth, phase and gain margin; appropriate selection of ω_c also helps to widen the bandwidth and reduce the sensitivity towards slight frequency variation; k_r can be tuned for shifting the response magnitude vertically without changing the bandwidth. If multiple frequencies need to be compensated, multiple resonant controllers can be integrated in one controller as illustrated by equation (16).

$$G(s)=k_p+\frac{k_rs}{s^2+\omega_n^2} \tag{14}$$

$$G(s)=k_p+\frac{2k_r\omega_cs}{s^2+2\omega_cs+\omega_n^2} \tag{15}$$

$$G(s)=k_p+\sum_{i=1}^{m}\frac{2k_{ri}\omega_{ci}s}{s^2+2\omega_{ci}s+\omega_i^2} \tag{16}$$

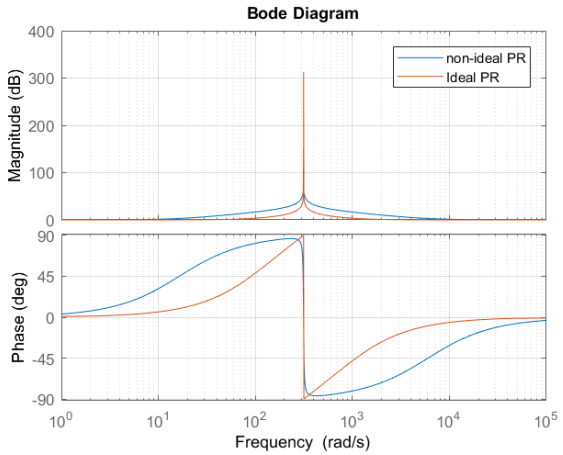

Fig.3 The bode plots of ideal and non-ideal PR controllers (k_p = 1, k_r = 1000, ω_c = 3 rad/s, ω_n = 314 rad/s)

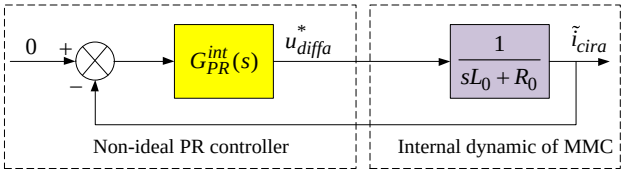

(a) Proposed control in phase *a*

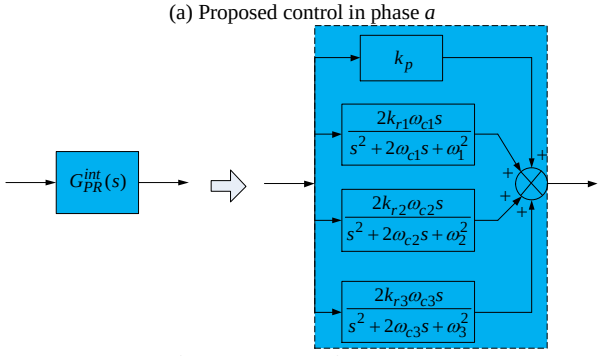

(b) Details of a three-resonant-frequency PR controller

Fig.4 The block diagrams of the proposed non-ideal PR controller

This article has been accepted for publication in a future issue of this journal, but has not been fully edited. Content may change prior to final publication. Citation information: DOI 10.1109/TEC.2019.2938395, IEEE Transactions on Energy Conversion

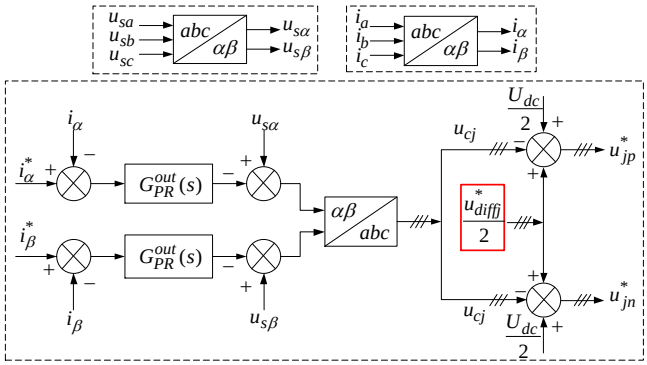

Fig.5 Overall control diagram of the MMC

According to the internal dynamic model of asymmetrical MMCs (see equation (13)), a three-resonant-frequency PR controller is designed, as shown by (17). The resonant frequencies are fundamental, 2nd and 3rd harmonic components, respectively, which can suppress the corresponding components in the circulating current.

$$G_{PR}^{int}(s) = k_p + \sum_{i=1,2,3} \frac{2k_{ri}\omega_{ci}s}{s^2 + 2\omega_{ci}s + \omega_i^2} \tag{17}$$

Combining (13) and (17), the non-ideal PR controller is illustrated in Fig.4. It can be observed that the inherent 2nd harmonic component and the fundamental and 3rd harmonic components caused by SM faults (asymmetrical internal structure) are suppressed by one single controller.

The overall control structure of a grid-connected MMC is shown in Fig.5, where a PR controller denoted by $G_{PR}^{out}(s)$ for the output AC current is utilized. The outputs of the proposed non-ideal PR controller (the red box) are added to the reference of the arm voltage.

B. *Parameter tuning*

As shown in Fig.4 (b), parameters k_p, k_{r1}, ω_{c1}, k_{r2}, ω_{c2}, k_{r3} and ω_{c3} need to be tuned. Taking one resonant frequency for instance, the open-loop transfer function (TF) of the internal dynamic of the MMC can be expressed by

$$G_{ol} = (k_p + \frac{2k_{r1}\omega_{c1}s}{s^2 + 2\omega_{c1}s + \omega_1^2}) \frac{1}{sL_0 + R_0} = \frac{k_p(s^2 + 2\omega_{c1}s + \omega_1^2) + 2k_{r1}\omega_{c1}s}{(s^2 + 2\omega_{c1}s + \omega_1^2)(sL_0 + R_0)} \tag{18}$$

Thus, the closed-loop TF can be represented by

$$G_{cl} = \frac{G_{ol}}{1 + G_{ol}} = \frac{k_p(s^2 + 2\omega_{c1}s + \omega_1^2) + 2k_{r1}\omega_{c1}s}{(sL_0 + R_0 + k_p)(s^2 + 2\omega_{c1}s + \omega_1^2) + 2k_{r1}\omega_{c1}s} \tag{19}$$

The basic design principle of the non-ideal PR controller is to decouple the proportional portion and resonant portions in the frequency domain, which allows them to be studied independently. Therefore, to determine the proportional gain of the controller, the closed-loop TF can be redefined for $k_{r1} = 0$ and $R_0 = 0$ (ignore the resistance of the arm inductance), leading to

$$G_{cl} = \frac{k_p / L_0}{s + k_p / L_0} \tag{20}$$

Based on equation (20), the bandwidth of the first-order system is found to be $\alpha_p = k_p / L_0$. k_p can be determined by selecting an appropriate bandwidth and phase angle. Equation (20) represents the dynamic of the system disregarding the impact that the resonant terms of the controller have over system stability.

A simple inspection shows that the dimension of K_r is angular frequency times impedance, or equivalently, angular frequency squared times inductance. The following parametrization gives the correct dimension.

$$K_r = 2k_{r1}\omega_{c1} = 2\alpha_r\alpha_p L_0 \tag{21}$$

Substituting (21) and $\alpha_p = k_p / L_0$ into (19) yields

$$G_{cl} = \frac{\alpha_p(s^2 + 2\alpha_r s + \omega_1^2)}{(s + \alpha_p)(s^2 + 2\alpha_r s + \omega_1^2) - 2\alpha_r s^2} \tag{22}$$

which can be approximated as

$$G_{cl} \approx \frac{\alpha_p(s^2 + 2\alpha_r s + \omega_1^2)}{(s + \alpha_p)(s^2 + 2\alpha_r s + \omega_1^2)} = \frac{\alpha_p}{s + \alpha_p} \tag{23}$$

Provided that the last term in the denominator of G_{cl} in equation (22) can be neglected, equation (23) is simplified to the closed-loop TF shown in equation (20). The approximation holds if

$$\alpha_r << \alpha_p \tag{24}$$

Hence, to satisfy equation (24), selecting $\alpha_r = 0.05\alpha_p$ gives

$$K_r = 0.1\alpha_p k_p \tag{25}$$

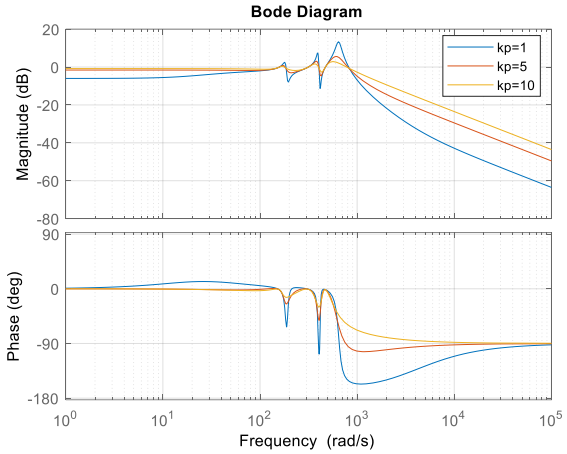

Fig.6 The bode plots of a closed-loop system with the proposed control

Therefore, selecting an appropriate ω_{c1} yields a corresponding k_{r1} based on equation (21) and equation (25). Fig.6 illustrates the corresponding bode plots based on different proportional terms (from 1 to 10).

V. Simulation Results

To verify the proposed control strategy, a three-phase 61-level MMC system is simulated using PSCAD/EMTDC, as shown in Fig.7. The parameters of the control and main circuits are shown in Tables II and III. The simulation process is designed as follows: from t = 0s to t = 0.25s, the MMC works under the normal condition with a conventional circulating current controller; during t = 0.25s to t = 0.45s, 3 (5% of the nominal sub-module number) SMs of the upper arm in phase a happen to be faulty without the proposed control; during t = 0.55s to t = 1s, the faulty SMs are still bypassed, and the proposed control is enabled. In addition, there is a power reversal (from P = -30MW to P = 30MW) at t = 0.65s.

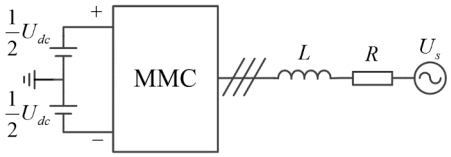

Fig.7 The single line diagram of the simulation model

TABLE II
CONTROLLER PARAMETERS IN SIMULATION

Symbol	Value	Symbol	Value	Symbol	Value
k_{r1}	200	k_{r2}	800	k_{r3}	600
ω_{c1}	2.5	ω_{c2}	2.5	ω_{c3}	2.5
k_p	5				

TABLE III
MAIN CIRCUIT PARAMETERS IN SIMULATION

Items	Symbol	Value
Rated AC line-to-line voltage	u_s	30 kV
AC system inductance	L	5 mH
AC system resistance	R	0.03 ohm
Rated frequency	f	50 Hz
Rated direct voltage	U_{dc}	60 kV
Arm inductance	L_0	15 mH
Equivalent arm resistance	R_0	1 ohm
Total number of SMs per arm	N	63
Number of redundant SMs per arm	N_r	3
Number of faulty SMs per arm	N_f	3
Capacitor voltage	U_c	1 kV
SM capacitance	C	8000 μF

A. *Case I*

The steady-state performance of the control strategy is shown in Fig.8. In this case, 3 SM faults occur at t = 0.25s, and are bypassed simultaneously. Since t = 0.55s, the proposed control method is enabled. The DC current is illustrated in Fig.8(a). It is easily seen that due to internal asymmetrical SM faults, the dc current fluctuates with the fundamental frequency. After enabling the proposed control, the DC fluctuation is entirely suppressed. Fig.8(b) and Fig.8(c) show the capacitor voltages of SM #1 and the arm currents in both upper and lower arms of phase *a*, respectively. It can be observed that the capacitor voltages and arm currents are affected little by the SM faults because only 5% of the SMs are bypassed. Fig.8(d) illustrates the circulating current of phase *a*, where the conventional controller can suppress the harmonics in the circulating current in the normal condition, but cannot eliminate all the components under SM faults; after enabling the proposed method, all harmonic components are eliminated. Finally, the three-phase AC currents, as provided in Fig.8(e), show that SM faults have little adverse effect on the AC currents.

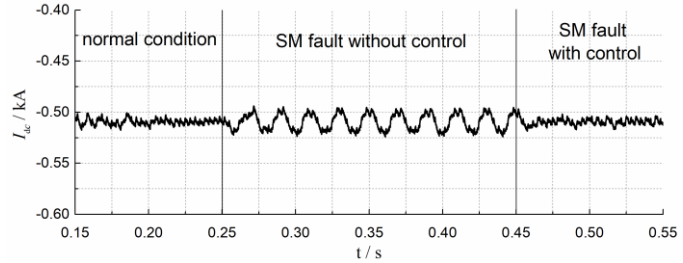

(a) DC current

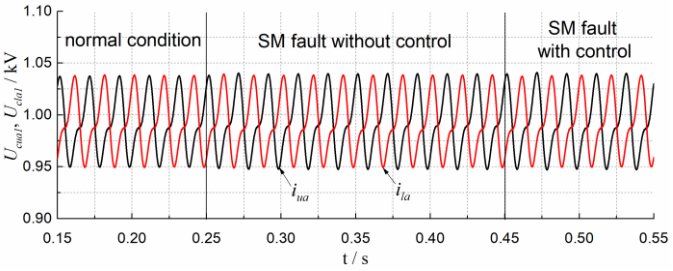

(b) SM capacitor voltages of phase *a*

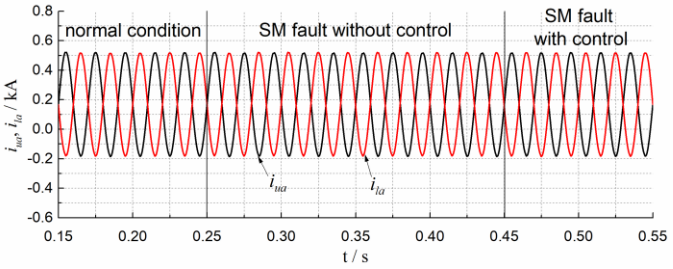

(c) Arm currents of phase *a*

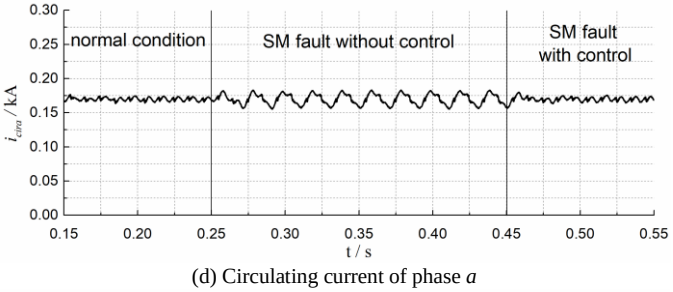

(d) Circulating current of phase *a*

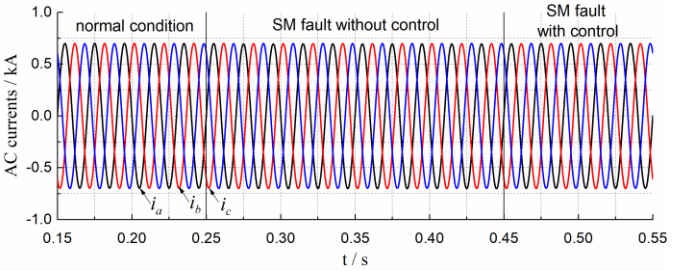

(e) Three-phase AC currents

Fig.8 The steady-state performance of the proposed controller

B. *Case II*

To verify the transient stability and response performance of the proposed control, an active power reversal is performed and zero reactive power is transferred under the SM-fault condition with the proposed control. A power reversal (-30MW to 30MW) occurs with 3 SM faults in the upper arm of phase *a* at t = 0.65s with the proposed control enabled. Fig.9 illustrates the detailed transient performance. Fig.9(a) shows that the DC current responses quickly without fundamental ripples. The capacitor voltages of SM #1 in the upper and lower arms remain stable after a quick transient process as shown in Fig.9(b). Fig.9(c) shows that the arm currents of phase *a* remain balanced after a step response. Fig.9(d) shows that the circulating currents of phase *a* have a fast and stable transient response during the transient process. Fig.9(e) illustrates that the three-phase AC currents have phase mutations when the active power changes from -30MW to 30MW. Active power and reactive power are shown in Fig.9(f), where it can be seen that SM faults only have slight impacts on active and reactive power.

This article has been accepted for publication in a future issue of this journal, but has not been fully edited. Content may change prior to final publication. Citation information: DOI 10.1109/TEC.2019.2938395, IEEE Transactions on Energy Conversion

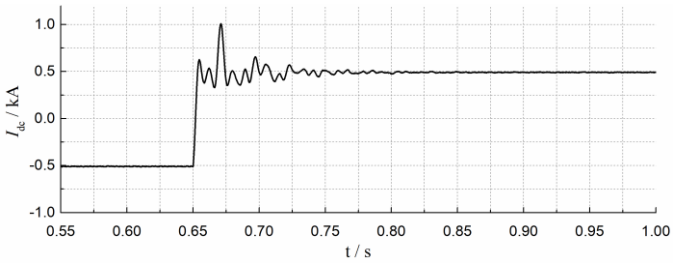

(a) DC current

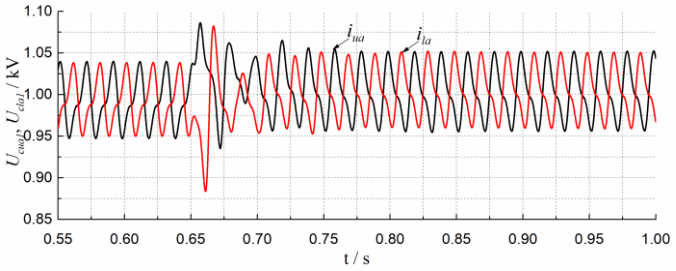

(b) SM capacitor voltages of phase *a*

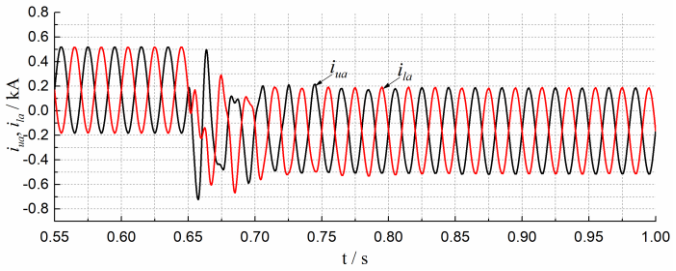

(c) Arm currents of phase *a*

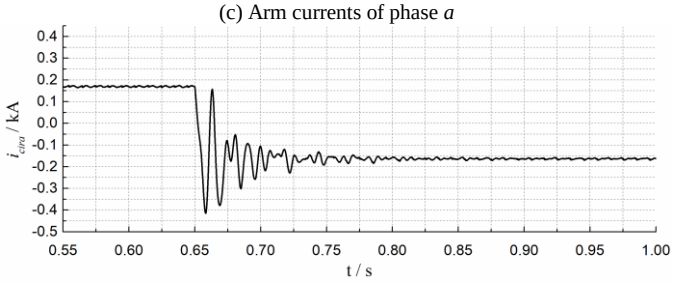

(d) Circulating current of phase *a*

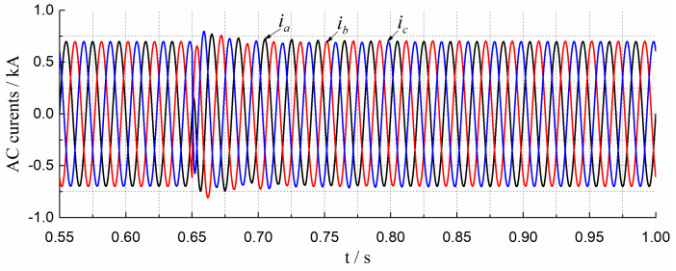

(e) Three-phase AC currents

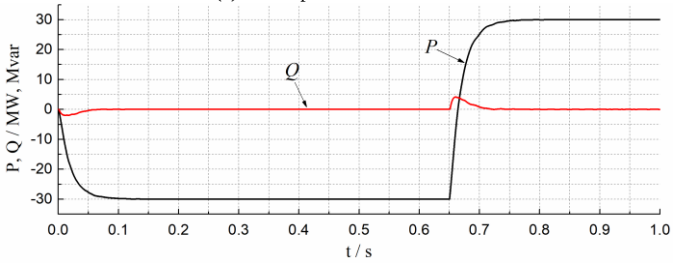

(f) Active and reactive power

Fig.9 The transient performance of the proposed controller

VI. EXPERIMENTAL RESULTS

The circuit scheme of the three-phase MMC prototype is illustrated in Fig.10, in which a pure resistive load is used to validate the control scheme. The photographs of the prototype are shown in Fig.11. The parameters of the main circuit are listed in Table IV. The main circuit uses MOSFETs as its power devices. A two-layer control structure is implemented by FPGA (EP3C80F484C8N) and NI Compact RIO (9022). Optical fibers are used to transmit necessary signals (i.e. trigger pulses, SM capacitor voltages and protection signals) between the main circuit and the control system.

To validate the control method, the following experimental procedures are designed. First, the prototype works in the normal situation (i.e. 44 SMs in an arm operate simultaneously, 4 of which work in hot-backup) until t = 1.2s when SMs #41–#44 in the upper arm of phase *a* are bypassed. Then, the prototype works without additional control in a 4-SM-fault situation during t = 1.2s to t = 1.4s. From t = 1.4s on, the proposed method is enabled finally.

TABLE IV
MAIN CIRCUIT PARAMETERS IN THE EXPERIMENT

Item	Symbol	Value
Rated AC bus line-line voltage	u_s	400 V
AC system inductance	L	9.6 mH
Rated frequency	f	50 Hz
Rated direct voltage	U_{dc}	800 V
Arm inductance	L_0	10 mH
Total number of SMs per arm	$N_{sumu,l}$	44
Number of redundant SMs per arm	N_r	4
Number of faulty SMs per arm	N_f	4
Rated capacitor voltage	U_d	20 V
Modulation index	m	0.9
Capacitance	C	4 mF

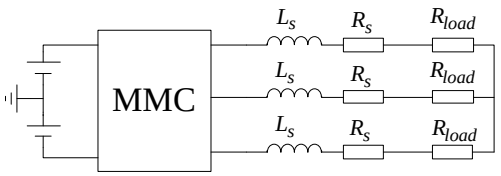

Fig.10 Experimental block diagram

Fig.11 The photographs of experimental setup

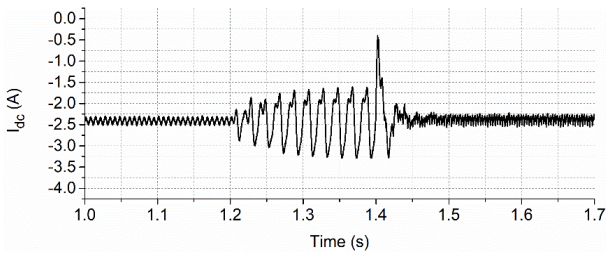

(a) DC current

This article has been accepted for publication in a future issue of this journal, but has not been fully edited. Content may change prior to final publication. Citation information: DOI 10.1109/TEC.2019.2938395, IEEE Transactions on Energy Conversion

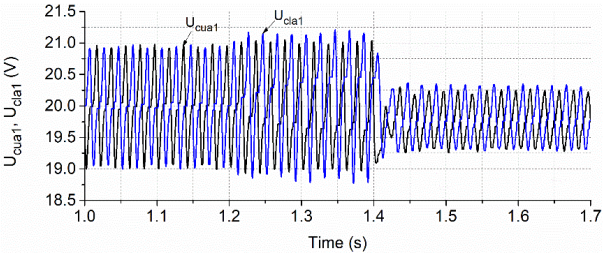

(b) SM capacitor voltages of phase *a*

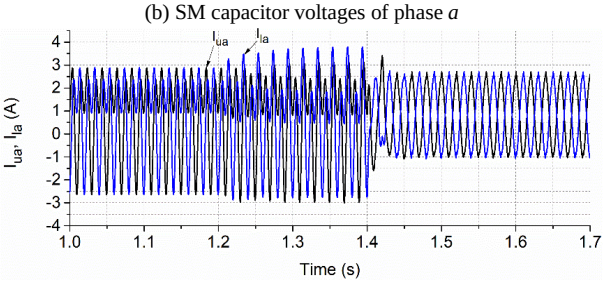

(c) Arm currents of phase *a*

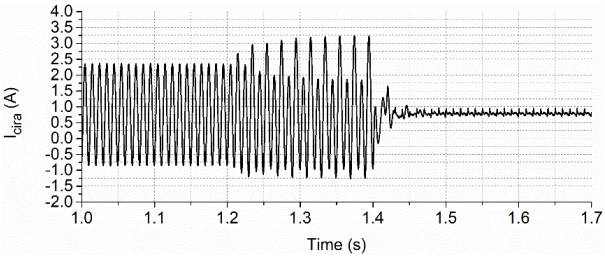

(d) Circulating current of phase *a*

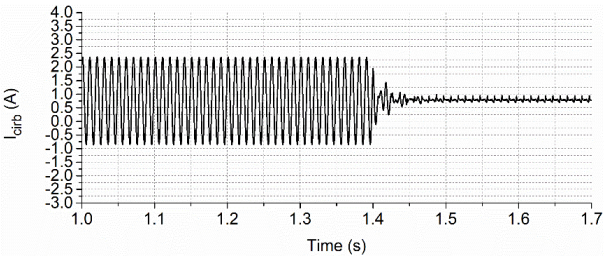

(e) Circulating current of phase *b*

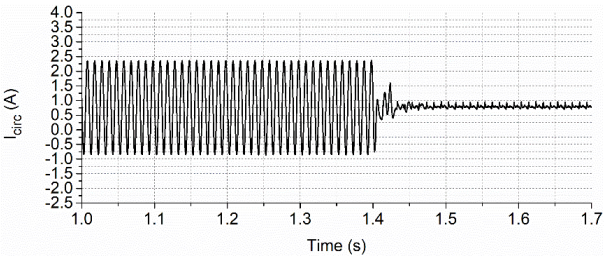

(f) Circulating current of phase *c*

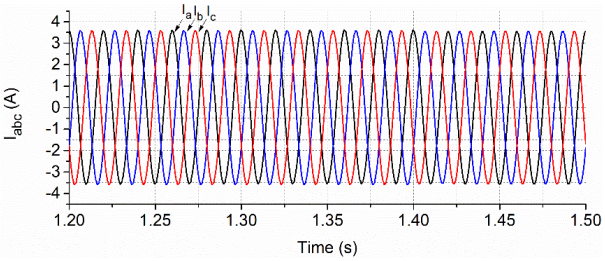

(g) AC currents

Fig.12 The experimental results of the proposed controller

It is worth mentioning that no circulating currents control is enabled during t = 1.2s to t = 1.4s so as to check the performance of the MMC without the circulating current controller under the normal and SM-fault conditions.

Fig.12 illustrates the performance of the entire experimental process. As shown in Fig.12(a), the peak-to-peak ripple accounts for nearly 69% of the desired pure DC value in DC current from t = 1.2s to t = 1.4s. After enabling the proposed control, the ripple is almost suppressed. Additionally, the capacitor voltages of two different SMs in the faulty phase (SM #1 of the upper arm and SM #1 of the lower arm) are shown in Fig.12(b), where imbalance appears during the faulty period without the proposed control and voltage ripples dramatically decrease after enabling the control. The arm currents and circulating current of phase *a* are shown in Fig.12(c) and (d). During t = 1.2s to t = 1.4s, the arm current becomes asymmetrical, resulting in the fundamental and 3rd harmonic components in the circulating current. From t = 1.4s on, the undesired phenomenon in the arm currents and circulating current of phase *a* disappears due to the proposed control. Fig.12(e)–(g) illustrate the circulating currents of phase *b* and phase *c* as well as the three-phase AC currents, respectively. The healthy phases suffer little from the faulty phase, and the three-phase AC currents suffer little from internal asymmetry. Besides, the 2nd harmonic components of the circulating currents of phases *b* and *c* are eliminated by the proposed control. In summary, the experimental results validate the effectiveness of the proposed PR controller no matter for the faulty or healthy phases.

VII. Conclusion

In this paper, redundant SMs are configured in hot-backup states, which helps to improve the reliability of MMCs. On this condition, a non-ideal proportional-resonant controller is designed by integrating the inherent circulating current suppression function and the SM-fault tolerant function. Owing to the bypass of the faulty SMs, MMCs work under internal asymmetry. By analyzing the internal asymmetrical dynamic model, it is found that fundamental, 2nd and 3rd harmonic components exist in the circulating current, and unbalanced circulating current results in fundamental ripples in DC current. A non-ideal PR controller is proposed to eliminate the corresponding AC components as well as the ripple of the DC current, whose effectiveness is validated by both simulation and experimental results.

Acknowledgment

This work was partially supported by the Fundamental Research Funds for the Central Universities, Project No. ZYGX2016KYQD138 and State Grid (SG) Fujian Electric Power Company Science and Technology Project (SGFJJY00GHJS1700061). The authors would like to gratefully acknowledge the financial support from China Scholarship Council.

References

[1]. Lesnicar, A. and R. Marquardt. An innovative modular multilevel converter topology suitable for a wide power range, in Power Tech Conference Proceedings, 2003 IEEE Bologna. 2003.

[2]. Allebrod, S., R. Hamerski and R. Marquardt. New transformerless, scalable Modular Multilevel Converters for HVDC-transmission, in

Power Electronics Specialists Conference, 2008. PESC 2008. IEEE. 2008.
[3]. P. Hu, and D. Jiang, A Level-Increased Nearest Level Modulation Method for Modular Multilevel Converters, IEEE Transactions on Power Electronics, vol. 30, no. 4, 2015, pp. 1836-1842.
[4]. Korn, A.J., M. Winkelnkemper and P. Steimer. Low output frequency operation of the Modular Multi-Level Converter, in Energy Conversion Congress and Exposition (ECCE), 2010 IEEE. 2010.
[5]. Ilves, K.; Antonopoulos, A.; Norrga, S.; Nee, H-P., "A New Modulation Method for the Modular Multilevel Converter Allowing Fundamental Switching Frequency," Power Electronics, IEEE Transactions on, vol.27, no.8, pp.3482-3494, Aug. 2012
[6]. Guan, M.; Xu, Z., "Modeling and Control of a Modular Multilevel Converter-Based HVDC System Under Unbalanced Grid Conditions," Power Electronics, IEEE Transactions on, vol.27, no.12, pp.4858-4867, Dec. 2012
[7]. Gum, T.S., et al., Design and Control of a Modular Multilevel HVDC Converter with Redundant Power Modules for Noninterruptible Energy Transfer. Power Delivery, IEEE Transactions on, 2012. 27(3): p. 1611-1619.
[8]. J. Guo, D. Jiang, Y. Zhou, P. Hu, Z. Lin, and Y. Liang, Energy storable VSC-HVDC system based on modular multilevel converter, INTERNATIONAL JOURNAL OF ELECTRICAL POWER & ENERGY SYSTEMS, vol. 78, 2016, pp. 269-276.
[9]. Adam, G.P., et al. Transformerless STATCOM based on a five-level modular multilevel converter, in Power Electronics and Applications, 2009. EPE '09. 13th European Conference on. 2009.
[10]. Hagiwara, M., R. Maeda and H. Akagi. Negative-sequence reactive-power control by a PWM STATCOM based on a modular multilevel cascade converter (MMCC-SDBC). in Energy Conversion Congress and Exposition (ECCE), 2011 IEEE. 2011.
[11]. Antonopoulos, A., et al. On interaction between internal converter dynamics and current control of high-performance high-power AC motor drives with modular multilevel converters, in Energy Conversion Congress and Exposition (ECCE), 2010 IEEE. 2010.
[12]. Hagiwara, M., K. Nishimura and H. Akagi, A Medium-Voltage Motor Drive with a Modular Multilevel PWM Inverter. Power Electronics, IEEE Transactions on, 2010. 25(7): p. 1786-1799.
[13]. Li, Z.; Wang, P.; Zhu, H.; Chu, Z.; Li, Y.; , "An Improved Pulse Width Modulation Method for Chopper-Cell-Based Modular Multilevel Converters," Power Electronics, IEEE Transactions on, vol.27, no.8, pp.3472-3481, Aug. 2012
[14]. W. Liu, K. Zhang, X. Chen and J. Xiong, "Simplified model and submodule capacitor voltage balancing of single-phase AC/AC modular multilevel converter for railway traction purpose," in IET Power Electronics, vol. 9, no. 5, pp. 951-959, 4 20 2016.
[15]. P. Hu, R. Teodorescu, S. Wang, S. Li and J. M. Guerrero, "A Currentless Sorting and Selection based Capacitor-Voltage-Balancing Method for Modular Multilevel Converters," in IEEE Transactions on Power Electronics. (in press)
[16]. Lin Wang, Ping Wang, Zixin Li and Yaohua Li, "A novel capacitor voltage balancing control strategy for modular multilevel converters (MMC)," 2013 International Conference on Electrical Machines and Systems (ICEMS), Busan, 2013, pp. 1804-1807.
[17]. Huiyu Miao, Jun Mei, Jianyong Zheng, Tian Ma and Chenyu Zhang, "A new MMC control strategy based on One-Cycle-Control and capacitor voltage balance," 2015 IEEE 2nd International Future Energy Electronics Conference (IFEEC), Taipei, 2015, pp. 1-5.
[18]. J. Sun, H. Liu, "Impedance modeling and analysis of modular multilevel converters", Proc. IEEE COMPEL Workshop, pp. 1-9, Jun. 2016.
[19]. Q. Song, W. Liu, X. Li, H. Rao, S. Xu and L. Li, "A Steady-State Analysis Method for a Modular Multilevel Converter," in IEEE Transactions on Power Electronics, vol. 28, no. 8, pp. 3702-3713, Aug. 2013.
[20]. L. Harnefors, A. Antonopoulos, S. Norrga, L. Angquist and H. Nee, "Dynamic Analysis of Modular Multilevel Converters," in IEEE Transactions on Industrial Electronics, vol. 60, no. 7, pp. 2526-2537, July 2013.
[21]. J. Sun and H. Liu, "Sequence Impedance Modeling of Modular Multilevel Converters," in IEEE Journal of Emerging and Selected Topics in Power Electronics, vol. 5, no. 4, pp. 1427-1443, Dec. 2017.
[22]. S. Rohner, S. Bernet, M. Hiller, and R. Sommer, “Modelling, simulation and analysis of a modular multilevel converter for medium voltage applications,” in Proc. IEEE Int. Conf. Ind. Technol., Vina del Mar, Chile, 2010, pp. 775-782
[23]. A. Lesnicar, “Neuartiger, modularer mehrpunktumrichter M2C für netzkupplungsanwendungen,” Ph.D. dissertation, Dept. Elect. Eng. Inf. Technol., Univ. of Bundeswehr, Munich, Germany.
[24]. Q. Tu, Z. Xu, H. Huang, and J. Zhang, “Parameter design principle of the arm inductor in modular multilevel converter based HVDC,” in Proc. Int. Conf. Power Syst. Technol., Hangzhou, China, 2010, pp
[25]. Q. Tu, Z. Xu and L. Xu, "Reduced Switching-Frequency Modulation and Circulating Current Suppression for Modular Multilevel Converters," in IEEE Transactions on Power Delivery, vol. 26, no. 3, pp. 2009-2017, July 2011.
[26]. Y. Zhou, D. Jiang, J. Guo, P. Hu and Y. Liang, "Analysis and Control of Modular Multilevel Converters Under Unbalanced Conditions," in IEEE Transactions on Power Delivery, vol. 28, no. 4, pp. 1986-1995, Oct. 2013.
[27]. S. Li, X. Wang, Z. Yao, T. Li and Z. Peng, "Circulating Current Suppressing Strategy for MMC-HVDC Based on Nonideal Proportional Resonant Controllers Under Unbalanced Grid Conditions," in IEEE Transactions on Power Electronics, vol. 30, no. 1, pp. 387-397, Jan. 2015.
[28]. M. Zhang, L. Huang, W. Yao, and Z. Lu, “Circulating harmonic current elimination of a CPS-PWM-based modular multilevel converter with a plug-in repetitive controller,” IEEE Trans. Power Electron., vol. 29, no. 4, pp. 2083–2097, Apr. 2014
[29]. B. Li, D. Xu, and D. Xu, “Circulating current harmonics suppression of modular multilevel converter based on repetitive control,” J. Power Electron., vol. 14, no. 6, pp. 1100–1108, Nov. 2014.
[30]. G. Konstantinou, J. Pou, S. Ceballos, R. Picas, J. Zaragoza, and V. G. Agelidis, “Control of circulating currents in modular multilevel converters through redundant voltage levels,” IEEE Trans. Power Electron., vol. 31, no. 11, pp. 7761–7769, Nov. 2016
[31]. J. Wang, H. Ma and Z. Bai, "A Submodule Fault Ride-Through Strategy for Modular Multilevel Converters With Nearest Level Modulation," in IEEE Transactions on Power Electronics, vol. 33, no. 2, pp. 1597-1608, Feb. 2018.
[32]. S. Shao, P. Wheeler, J. Clare, and A. Watson, “Fault detection for modular multilevel converters based on sliding mode observer,” IEEE Trans. Power Electron., vol. 28, no. 11, pp. 4867–4872, Nov. 2013.
[33]. Y. Feng, J. Zhou, Y. Qiu, and K. Feng, “Fault tolerance for wind turbine power converter,” in Proc. 2nd IET Renew. Power Gen. Conf., Beijing, China, Sep. 9–11, 2013, pp. 1–4.
[34]. F. Deng, Z. Chen, M. K. Rezwan, and R. Zhu, “Fault detection and localization method for modular multilevel converters,” IEEE Trans. Power Electron., vol. 30, no. 5, pp. 2721–2732, May 2015.
[35]. B. Li, S. Shi, B. Wang, G. Wang, W. Wang, and D. Xu, “Fault diagnosis and tolerant control of single IGBT open-circuit failure in modular multilevel converters,” IEEE Trans. Power Electron., vol. 31, no. 4, pp. 3165–3176, Apr. 2015.
[36]. P. Hu, D. Jiang, Y. Zhou, Y. Liang, J. Guo, and Z. Lin, “Energy-balancing control strategy for modular multilevel converters under submodule fault conditions,” IEEE Trans. Power Electron., vol. 29, no. 9, pp. 5021–5030, Sep. 2014.
[37]. F. Deng, Y. Tian, R. Zhu and Z. Chen, "Fault-Tolerant Approach for Modular Multilevel Converters Under Submodule Faults," in IEEE Transactions on Industrial Electronics, vol. 63, no. 11, pp. 7253-7263, Nov. 2016.
[38]. G. T. Son et al., "Design and Control of a Modular Multilevel HVDC Converter With Redundant Power Modules for Noninterruptible Energy Transfer," in IEEE Transactions on Power Delivery, vol. 27, no. 3, pp. 1611-1619, July 2012.
[39]. L. Harnefors, A. Antonopoulos, S. Norrga, L. Angquist and H. Nee, "Dynamic Analysis of Modular Multilevel Converters," in IEEE Transactions on Industrial Electronics, vol. 60, no. 7, pp. 2526-2537, July 2013.

Pengfei Hu (S’13-M’17) was born in Suining, China, on January 8, 1988. He received his B.E. and Ph.D. degrees in Electrical Engineering and Its Automation from the College of Electrical Engineering, Zhejiang University, Hangzhou, China, in 2010 and 2015, respectively. He is now working as an assistant professor in the University of Electronic Science and

Technology of China (UESTC). From Dec 2017 on, he is working as a visit professor in Aalborg University.

His research interests include high- voltage DC (HVDC) transmission, flexible AC transmission systems (FACTS), and DC distribution network.

Zhengxu He was born in Fuquan, China, on October 3, 1990. She received the B.E. degree and M.Eng degree in environmental engineering from Tsinghua University, Beijing, China in 2012 and 2015, respectively. She is currently with Sichuan Energy Internet Research Institute as a researcher.

Her research interests mainly include building energy efficiency, energy internet and internet of things.

Shuqi Li was born in Chengdu, China, on April 17, 1990. She received the B.E. degree and M.Eng. degree in electrical engineering from Shanghai Jiao Tong University (SJTU), Shanghai, China in 2012 and 2015, respectively. She is currently with State Grid Sichuan Electric Power Research Institute as an engineer.

Her research interests mainly include high-voltage dc transmission and dc distribution network.

Josep M. Guerrero (S'01-M'04-SM'08-FM'15) received the B.S. degree in telecommunications engineering, the M.S. degree in electronics engineering, and the Ph.D. degree in power electronics from the Technical University of Catalonia, Barcelona, in 1997, 2000 and 2003, respectively. Since 2011, he has been a Full Professor with the Department of Energy Technology, Aalborg University, Denmark, where he is responsible for the Microgrid Research Program (www.microgrids.et.aau.dk).

His research interests are oriented to different microgrid aspects, including power electronics, distributed energy-storage systems, hierarchical and cooperative control, energy management systems, smart metering and the internet of things for AC/DC microgrid clusters and islanded minigrids; recently specially focused on maritime microgrids for electrical ships, vessels, ferries and seaports.

Prof. Guerrero is an Associate Editor for the IEEE TRANSACTIONS ON POWER ELECTRONICS, the IEEE TRANSACTIONS ON INDUSTRIAL ELECTRONICS, and the IEEE INDUSTRIAL ELECTRONICS MAGAZINE, and an Editor for the IEEE TRANSACTIONS ON SMART GRID.